ORIGINAL ARTICLE

IN SILICO LIBRARY SCREENING TO FIND NOVEL ANTICANCER AGENT WITH CHEMOSENSITIZING PROPERTIES: FOCUS ON TARGETING ATAXIA TELANGIECTASIA AND Rad3 RELATED KINASE

Darina Muthna [1,#]**, Tomas Kucera** [2,#]**, Zbynek Vecera** [2]**, Lukas Gorecki** [3]**, Martin Andrs** [3]**, Martina Rezacova** [1 ✉]**, Jan Korabecny** [3 ✉]

[1] Department of Medical Biochemistry, Faculty of Medicine in Hradec Kralove, Charles University, Simkova 870, 500 38 Hradec Kralove, Czech Republic

[2] Department of Toxicology and Military Pharmacy, Trebesska 1575, 500 05 Hradec Kralove, Czech Republic

[3] Biomedical Research Center, University Hospital Hradec Kralove, Sokolska 581, 500 05 Hradec Kralove, Czech Republic

[#] Darina Muthna and Tomas Kucera contributed equally to this study.

Summary

To bypass the resistance to conventional chemotherapy, attention is paid to the inhibition of alternative targets such as members of the DNA damage response pathway. In the present study, we performed a three-step virtual screening of potential ATR inhibitors followed by evaluation of antiproliferative and chemosensitizing properties of selected compounds *in vitro* on a panel of cancer cell lines. According to pharmacophore resemblance to standard ATR inhibitor VX-970, a total of 17 compounds were purchased and tested. Among those 17 compounds, two proved antiproliferative efficacy in monotherapy, whereas ten compounds were effective in cisplatin co-treatment on the panel of ten different human cell lines.

Key words: In silico screening; drug development; ATR kinase; cancer treatment; chemosensitization

Introduction

Cancer imposes a global health problem with a significant mortality rate and increasing incidence worldwide. The number of new cases inexorably rises with population aging and exposure to risk factors (1). The treatment

Martina Rezacova

✉ Charles University, Faculty of Medicine in Hradec Kralove, Department of Medical Biochemistry, Simkova 870, 500 38 Hradec Kralove, Czech Republic

▭ rezacovam@lfhk.cuni.cz

☎ 00-420-495-816-295

Jan Korabecny

✉ University Hospital, Biomedical Research Centre, Sokolska 581, 500 05 Hradec Kralove, Czech Republic
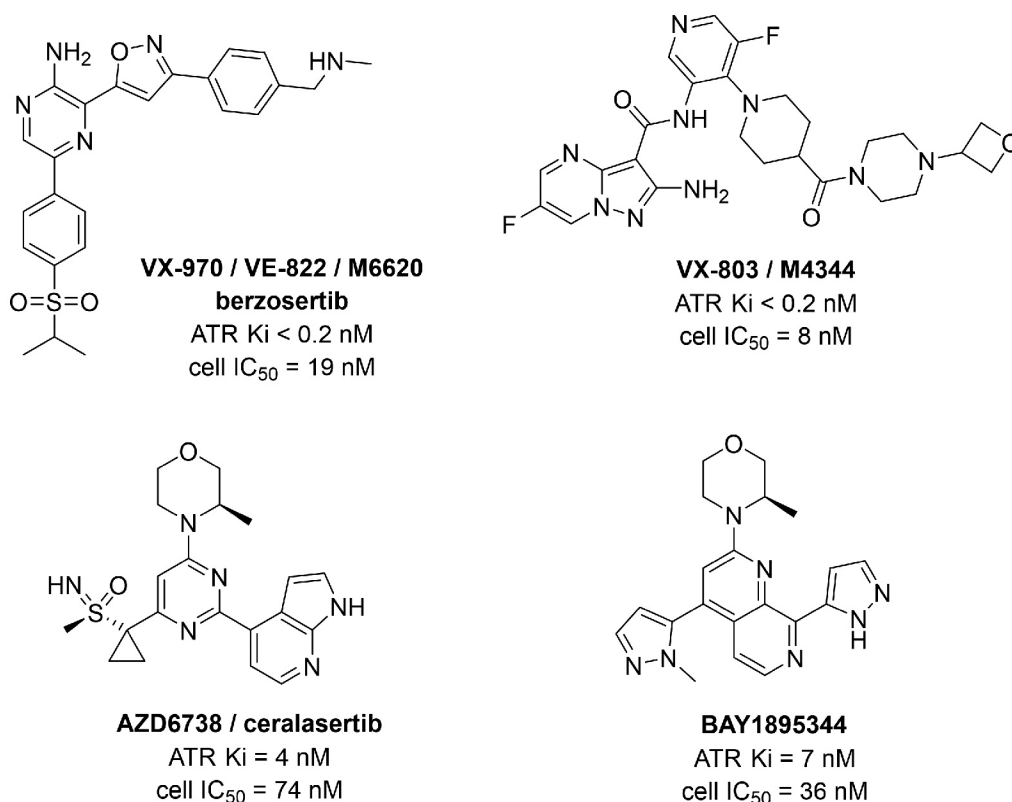
▭ jan.korabecny@fnhk.cz

☎ 00-420-495-833-447

of cancer represents one of the biggest challenges in modern medicine. The goal is to selectively kill cancerous cells, while sparing the healthy ones. To pursue that, we must aim at the hallmarks of cancer (2). Currently, cancer treatment mostly relies on surgical resection, radiation therapy, chemotherapy intervention, or targeted therapy. While surgical resection and targeted therapy are robust tools, they are not suitable for all patients. Most patients thus rely on broad-acting radiation and chemotherapy. Those modes of treatment exploit the sustained and uncontrolled proliferation and disrupted genome maintenance. Although different types of cancer are susceptible to chemotherapy, multimodal resistance to these agents is frequently occurring as a consequence of the evolutionary process (3). Such deliberate processes result from DNA mutations and metabolic changes in the affected cell lines to ensure their survival, for example, by activating cell cycle checkpoints, leading to the cell cycle arrest (4).

Different approaches have emerged to counteract the drug resistance depending on the acquired mechanism of resistance. To circumvent the phenomenon of resistance, research concentrated on alternative agents to DNA-damaging drugs such as ataxia telangiectasia and Rad3 related kinase (ATR) inhibitors that can target the DNA damage response signalling pathways (5). ATR is a serine-threonine kinase that, in co-action with ataxia telangiectasia mutated (ATM) and DNA-dependent protein kinase (DNA-PK), establish a backbone network responding to DNA-damage (6). All of these kinases are members of the phosphatidylinositol-3-kinase related kinase (PIKK) family. ATR is activated mainly during replication stress, but in general, it responds to a variety of DNA damage types, both endogenous and exogenous, e.g., from UV radiation, treatment with DNA cross-linking agents, or alkylating bases (7). Under physiological conditions, activated ATR facilitates DNA repair by S-phase slow down, and by G2/M cell cycle arrest via Checkpoint 1 (CHK1) kinase, preventing cells' progression into mitosis (6). The actions of ATM and DNA-PK are more restricted to the repair of DNA double-strand breaks (DSBs), the events caused by ionizing radiation (IR), or e.g., topoisomerase II inhibitors. Both, ATM and ATR kinases, share a high degree of structural homology with overlapping roles in maintaining cell survival. The function of ATM is frequently disrupted in tumor cells; complete loss of its activity is often associated with cancer progression and conventional therapy resistance (8). Moreover, the loss of ATM activity shifts the dependence for cell survival to other DNA damage repair kinases like ATR. Under these conditions, several studies have disclosed that cancerous cells exposed to DNA damaging agents are sensitive to ATR inhibition (9, 10). Accordingly, normal cells can tolerate ATR inhibition by compensatory mechanism orchestrated via ATM-mediated pathway (11). Large body of evidence also corroborates the monotherapy with ATR inhibitors for some types of tumors as well as combination therapy with other repair protein inhibitors like poly(ADP-ribose)polymerase (PARP) and CHK1 inhibitors (12–16). ATR inhibition lies on the borderline between chemotherapy and targeted therapy. On one side, it disrupts the response to DNA damage of all cells, on another it can exploit the defectiveness of various cancer types allowing selective targeting.

The finding that chemosensitizing agents enhance the cytotoxic potential of DNA-damaging agents preferably in cancer cells, motivated researchers in the field to actively search for new selective drugs to target DNA repair pathways in cancer cells (17). Out of them, ATR represents the target of particular interest since it is rarely mutated, its activity is triggered by most cancer chemotherapy strategies, and in tandem with frequently disrupted ATM/p53 pathway, ATR demonstrates synthetic lethal interactions (11, 18). The knowledge about ATR kinase gained so far has clearly pointed out that its inhibition can sensitize cancer cells to radio- or chemosensitizing insults with a high vulnerability rate directed to cancer cells while preserving healthy ones (19). All these findings support the role of ATR as a drugable kinase to aid combating highly aggressive and resistant hypoxic tumors (20, 21).

The current portfolio of ATR inhibitors developed by academia and pharmaceutical companies is relatively narrow (5, 22, 23). The challenges that are associated with their discovery can be classified as the difficulties in obtaining viable protein for the testing of potential ATR inhibitors, the lack of standardized screening methods, the scarcity of structural information related to ATR kinase, and highly conserved catalytic site among the members of PIKK family resulting mostly in low selectivity of the final entity. Despite challenging tasks, the known ATR kinase inhibitors were either identified from natural sources or developed by medicinal chemistry approaches, and are reviewed elsewhere (17, 23–25). To name a few, berzosertib (M6620/VX-970/VE-822), ceralasertib (AZD6738), M4344 (VX-803), and BAY1895344 (Fig. 1) are known most advanced clinical candidates with selective pattern to ATR inhibition (25).

VX-970 / VE-822 / M6620
berzosertib
ATR Ki < 0.2 nM
cell IC$_{50}$ = 19 nM

VX-803 / M4344
ATR Ki < 0.2 nM
cell IC$_{50}$ = 8 nM

AZD6738 / ceralasertib
ATR Ki = 4 nM
cell IC$_{50}$ = 74 nM

BAY1895344
ATR Ki = 7 nM
cell IC$_{50}$ = 36 nM

Figure 1. Chemical structure of ATR kinase inhibitors currently evaluated in the clinical trial testing.

Study design

Structure of ATR kinase complexed with ATR-interacting protein (ATRIP) has been elucidated by cryo-electron microscopy analysis at 4.7 Å resolution recently (26). The study disclosed that ATR is endowed with a large *N*-terminal α-solenoid-shaped coil, FAT and kinase domains, and a C-terminal short section known as FATC. Overall, the complex mimics a hollow heart shape from the front view.
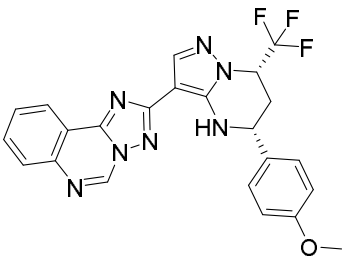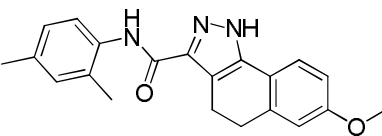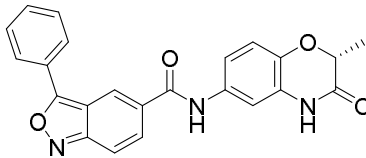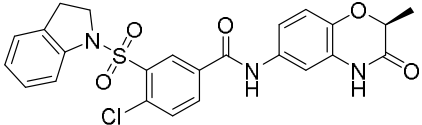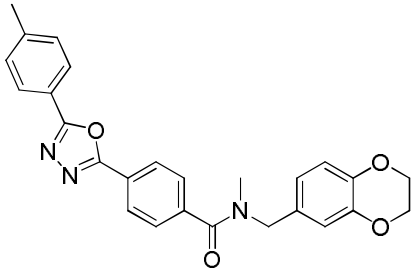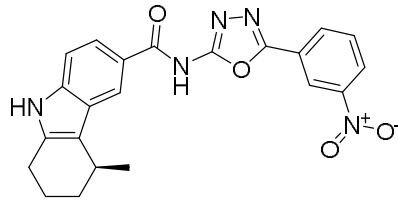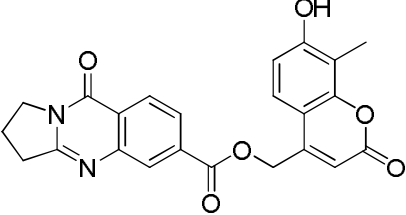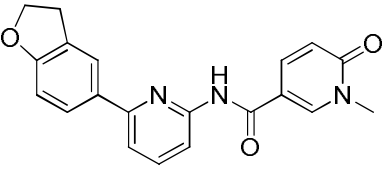
Our working hypothesis was built on the structural resemblance to the template scaffold VX-970. Studying the structural requirements predicted by ATR homology molecular modelling based on PI3Kγ kinase (PDB ID: 1E7V) (27), or docked ligand into ATR kinase domain of cryo-electron microscopy structure (PDB ID: 5YZ0) (26) revealed several critical interactions (Fig. 2). Indeed, VX-970 occupies a deep pocket dedicated to ATP binding where the substrate is phosphorylated. 2-Aminopyrazine moiety is lodged in the vicinity of the adenine-binding site of ATP. Herewith, the apparent hydrogen bonds were predicted between the amine group of 2-aminopyrazine and the backbone amide of Glu2378, *N1* pyrazine and amide group of Val2380 and parallel π-π stacking with Trp2379. Isoxazole heterocycle of VX-970 is nested close to the ribose-binding site of ATP contacting hydroxyl group of Tyr2365 residue. Protonated terminal secondary amine of VX-970 forms several hydrogen bonds with oxygens from Asp2330, Asn2480, and carboxyl group of Asp2494. Isopropylsulfonyl group of VX-970 is merged with the phosphate group of ATP, displaying interaction with Gly2385. All the highlighted interactions have been considered as critical aspects in the search for novel potential inhibitors in the current study. To this end, we have applied a sequential virtual screening campaign using ZINC Purchasable ligand library (28). In the first step, we filtered 7,307 hits based on the pharmacophore resemblance to VX-970. The second phase included semi-flexible molecular modeling prediction selecting 293 compounds. In the last step, all the ligands underwent flexible docking studies with eight amino acid residues highlighting a total of 17 compounds that were purchased and tested (Table 1). The compounds were then evaluated for their cytotoxic potential compared to VE-821 using ten different cell lines. Chemosensitizing properties were evaluated with cisplatin co-treatment using different cell lines.
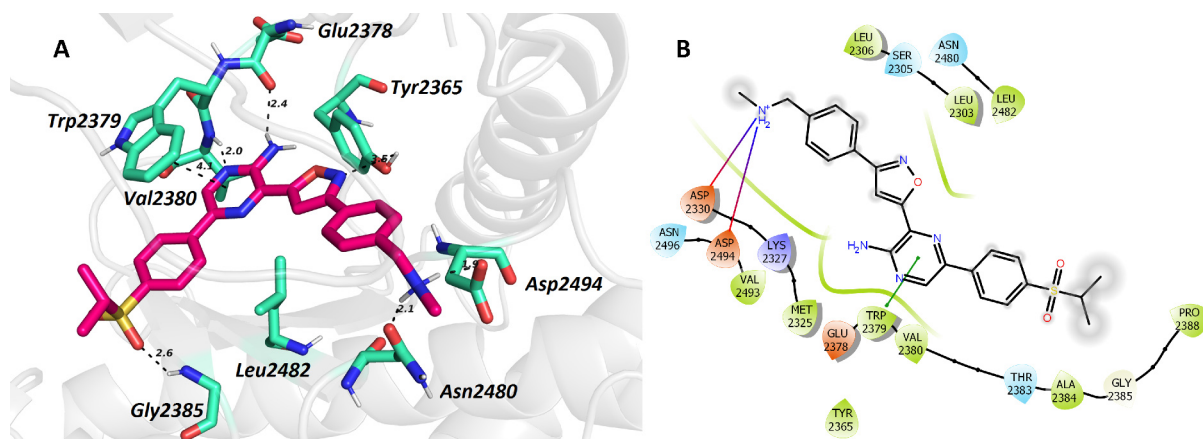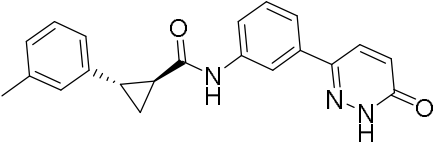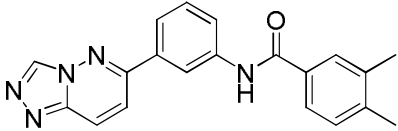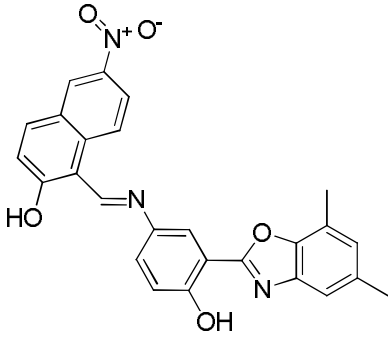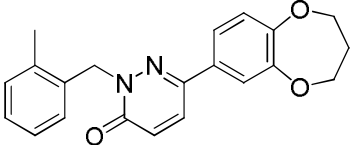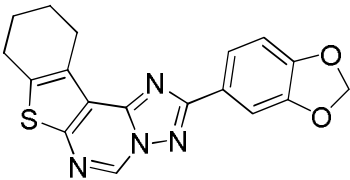
Figure 2. Predicted binding pose of VX-970 in ATR homology molecular modeling based on PI3Kγ kinase (PDB ID: 1E7) (27) with highlighted interactions between ligand and ATR kinase rendered as three- (A) or two-dimensional (B) representations.

Table 1. Compounds selected from ZINC database as potential ATR kinase inhibitors, their chemical structures, and calculated binding affinities by AutoDock Vina software.

Compound No.	ZINC code	Chemical structure	binding (kcal/mol)
1	ZINC02108997		-12.4
2	ZINC02196876		-10.9
3	ZINC02786769		-12.1
4	ZINC02806317		-12.3

5	ZINC02731435		-12.5
6	ZINC21018358		-11.2
7	ZINC09914417		-11.9
8	ZINC09459851		-12.4
9	ZINC9585571		-11.9
10	ZINC6946633		-12.3
11	ZINC40159284		-12.1
12	ZINC71888365		-11.4

| 13 | ZINC69418748 | | -11.2 |
14	ZINC05168622		-11.0
15	ZINC254812573		-12.0
16	ZINC63863963		-10.9
17	ZINC02436075		-10.9

Results and Discussion

Identification of new hits using in silico screening

Our three-step protocol identified 17 novel potential ATR inhibitors (Table 1). Indeed, all the compounds to some extent mimics the binding pattern of VX-970 occupying the ATP binding pocket of ATR kinase (Figures 3-6). Closer exploration revealed that 3*H*-benzo[*f*]chromen-3-one moiety from **1** (Fig. 3A) is anchored via π-π stacking to Trp2379 in adenine binding pocket of ATP. Besides, Val2380 is also engaged in ligand binding by hydrogen bond to heterocyclic oxygen of 3*H*-benzo[*f*]chromen-3-one moiety. 1 also protrudes towards the ribose binding site of ATP, forming hydrogen contact with hydroxyl of Tyr2365. Similarly, compound **2** is nested in the vicinity of Trp2379 (Fig. 3B). [1,2,4]Triazolo[3,4-*a*]phthalazine ring centres the ligand towards Tyr2365. In a slightly different manner, compound **3** accommodated the ATP binding pocket of ATR, but preserving the critical hydrophobic interaction (Fig. 3C). The most peculiar interaction observed is the hydrogen bond between 1,2,4-triazole and Lys2327. Docking studies also highlighted a very similar analogue of **3**, namely **4** (Fig. 3D), that generally demonstrated very close binding occupancy to that of **3** around Lys2327, but the rest of the molecule is 180°rotated.
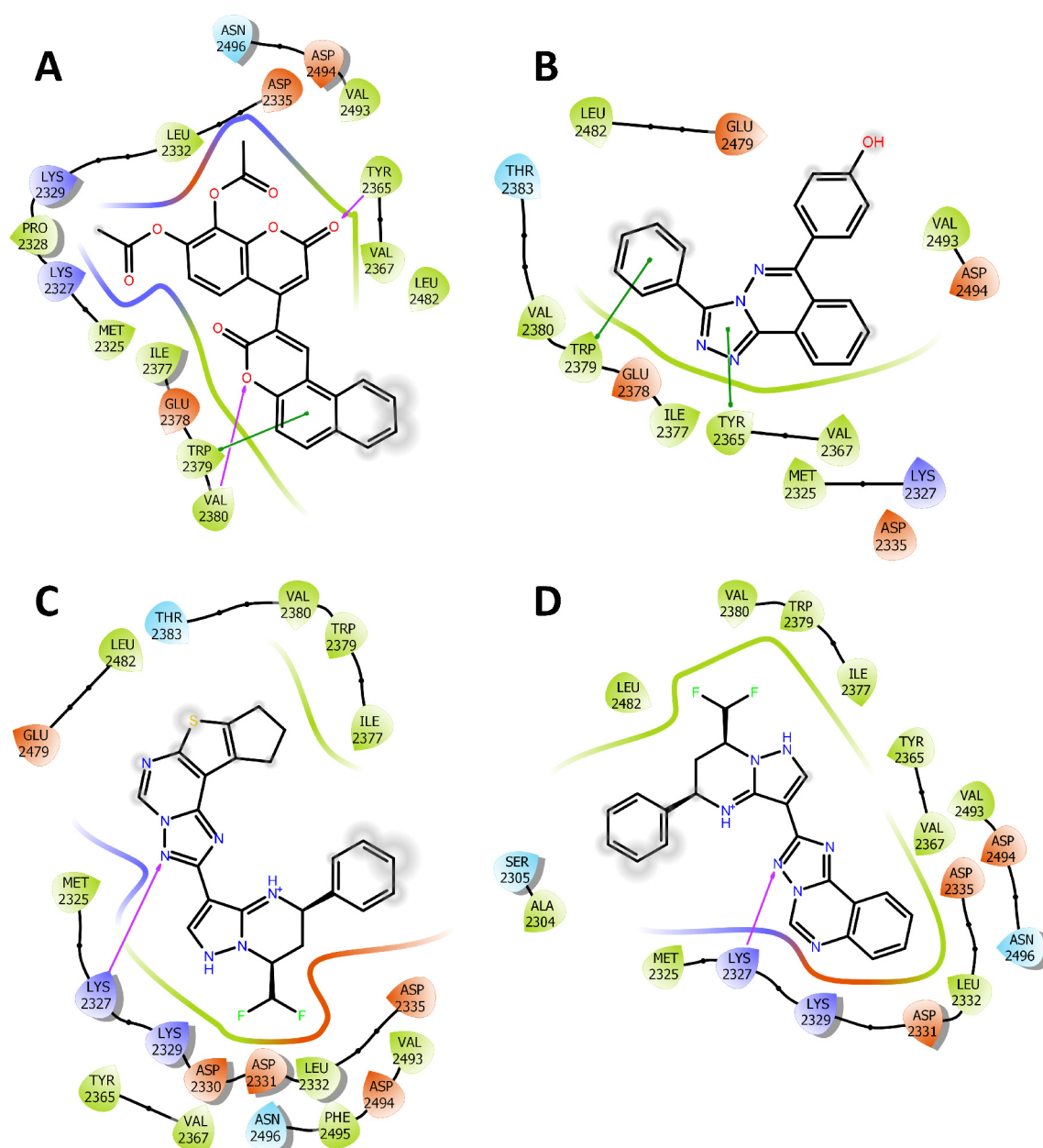
Figure 3. Two-dimensional representation of ligands **1-4** (A-**1**, B-**2**, C-**3**, D-**4**) bound to ATP-binding pocket of ATR kinase. Negatively charged area is colored by red residues or contour surrounding them, positively charged area by dark blue, hydrophobic interaction in green, polar interaction in light blue, solvent exposure via grey color, π-π stacking in green line between the residue and the ligand, cation-π in red line between the residue and the ligand, and hydrogen bond is displayed by the single-oriented purple arrow. The figure was created by Maestro v. 11.4 (Schrödinger, LLC, New York, NY, 2017).

Another 1,2,4-triazole-containing analogue **5** is also anchored to Lys2327 (Fig. 4A). More importantly, Gly2385, usually binding the phosphate group of ATP, is implicated in contact with the ligand via van der Waals interaction. Trp2379 centrally accommodates *N*-(2,4-dimethylphenyl)acetamide of **6** (Fig. 4B). An interesting binding pattern was exerted by **7**, forming π-π contact between Trp2379 with 2,1-benzoxazole scaffold, hydrogen bond between amide group of **7** to Lys2327, and contact with Gly2385 (Fig. 4C). Several amino acid residues of ATR are presumably involved in binding ligand **8** (Fig. 4D). It accounts, among others, cation-π and π-π interactions with Lys2327 and Trp2379, respectively.
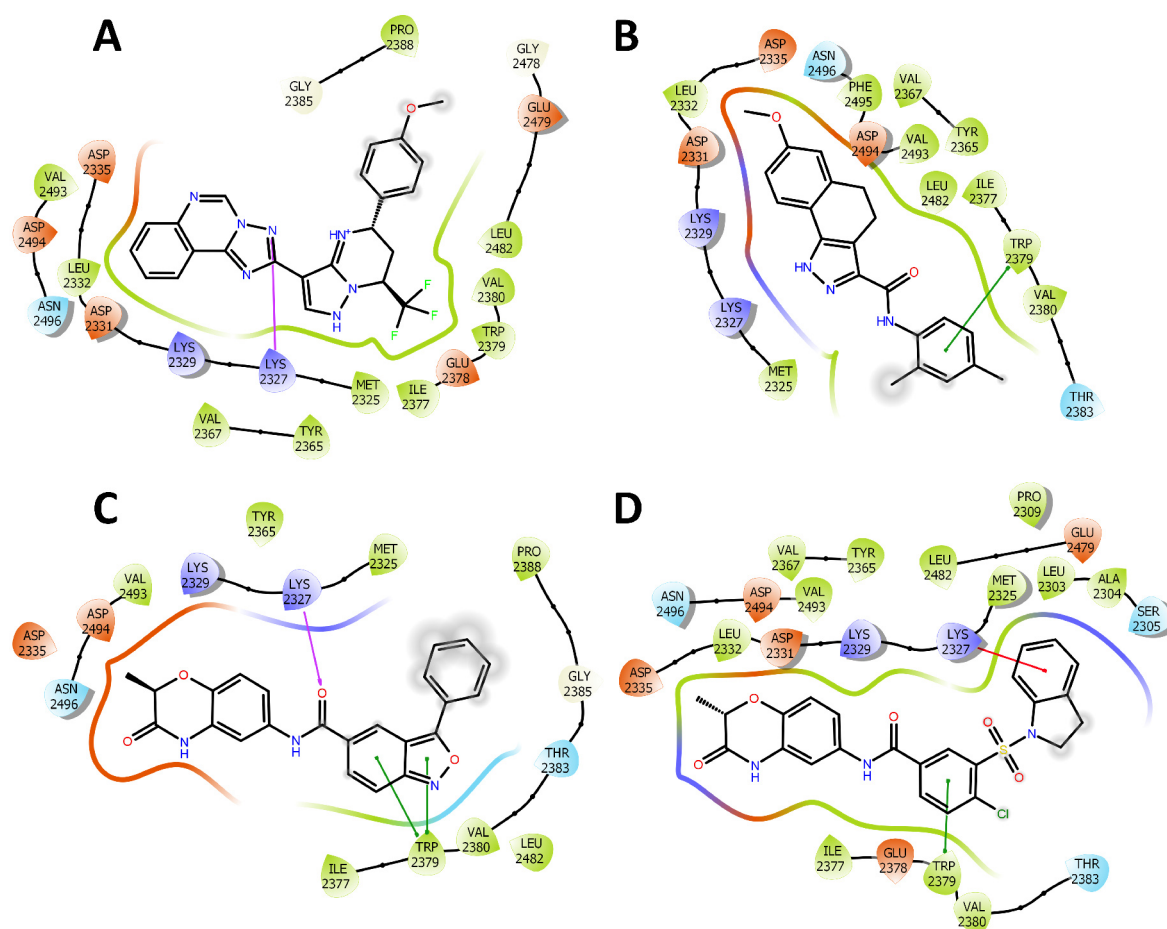
Figure 4. Two-dimensional representation of ligands **5-8** (A-**5**, B-**6**, C-**7**, D-**8**) bound to ATP-binding pocket of ATR kinase. Negatively charged area is colored by red residues or contour surrounding them, positively charged area by dark blue, hydrophobic interaction in green, polar interaction in light blue, solvent exposure via grey color, π-π stacking in green line between the residue and the ligand, cation-π in red line between the residue and the ligand, and hydrogen bond is displayed by the single-oriented purple arrow. The figure was created by Maestro v. 11.4 (Schrödinger, LLC, New York, NY, 2017).

In the case of **9** complexed with ATR, Trp2379 orchestrates tethering to ligand by π-π interactions with two different regions of **9**, namely 4-methylphenyl and 1,3,4-oxadiazole moieties mimicking the appendage of template VX-970 (Fig. 5A). Two lysine residues (Lys2327 and Lys2329) displayed cation-π contacts with terminal 2,3-dihydro-1,4-benzodioxine moiety of **9**. Moreover, oxygen from amide group generated hydrogen bond interaction with hydroxyl from Tyr2365 and amine from Asp2494. 3 Nitrobenzene moiety of **10** faces towards Trp2379, and its nitro group is implicated in hydrogen contact with Thr2383 (Fig. 5B). 3-Methyl-2,3,4,9-tetrahydro-1*H*-carbazole occupies ribose binding site of ATP in ATR active site, where Lys2327 established cation-π interaction with this moiety of **10**. Moreover, Asp2335 demonstrated hydrogen contact with secondary amine of carbazole heterocycle. The binding pattern of **11** is of particular interest since the ligand also spans the phosphate-binding site of ATP in ATR kinase defined by Gly2385 (Fig. 5C). The drawback might be seen in not establishing the crucial interaction with Trp2379 from the adenine binding site of ATP. On the contrary, the interaction with Trp2379 is visible with 2,3-dihydro-1-benzofuran moiety in 12 (Fig. 5D). Notably, Tyr2365 plays a dual role in anchoring the ligand mediating the π-π stacking with pyridine ring as well hydrogen contact with closely attached amide group.

For the compound **13** (Fig. 6A), its methylphenyl moiety occupies the hydrophobic region of the kinase with the most apparent contact to Trp2379. The other pole of **13** is lodged to the ribose binding site of ATP, making
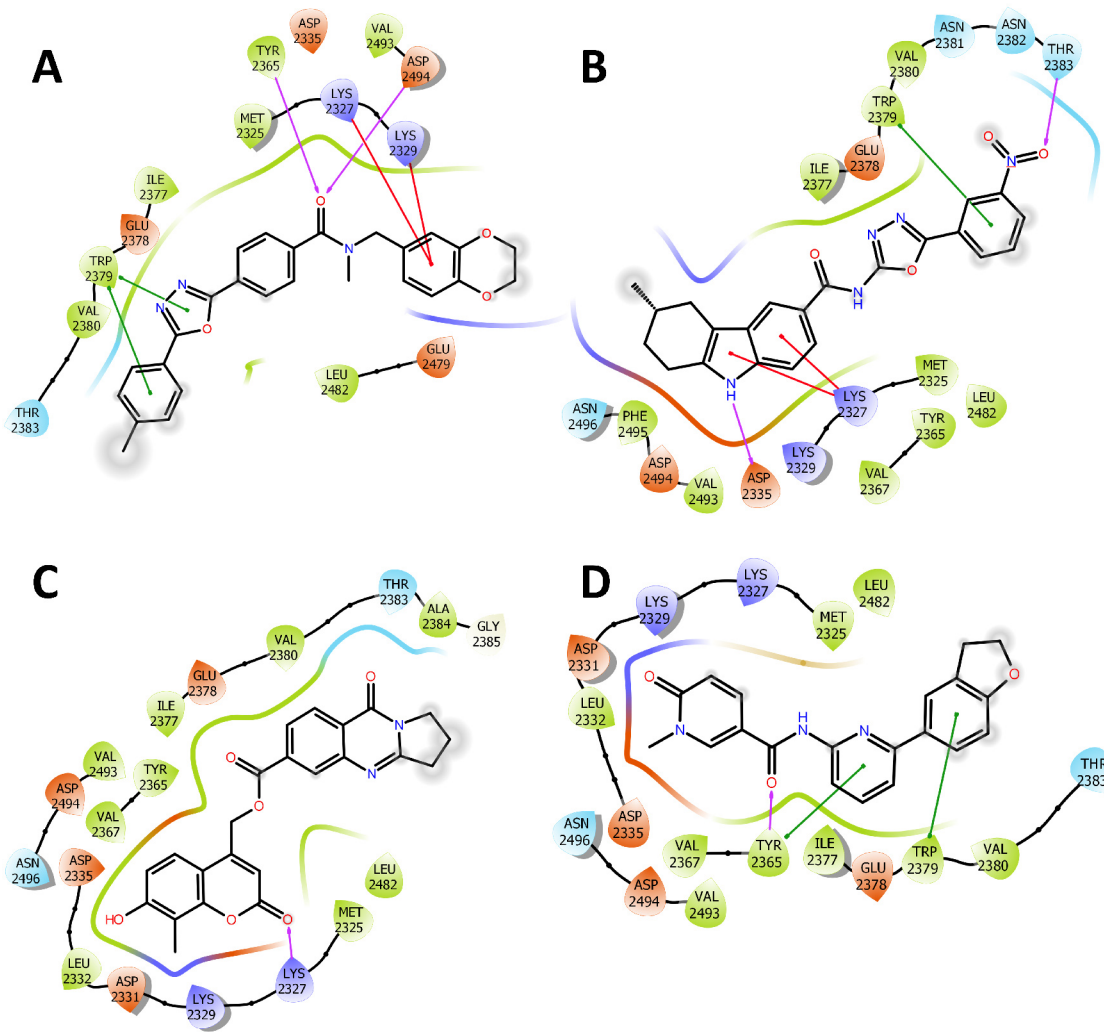
Figure 5. Two-dimensional representation of ligands **9-12** (A-**9**, B-**10**, C-**11**, D-**12**) bound to ATP-binding pocket of ATR kinase. Negatively charged area is colored by red residues or contour surrounding them, positively charged area by dark blue, hydrophobic interaction in green, polar interaction in light blue, solvent exposure via grey color, π-π stacking in green line between the residue and the ligand, cation-π in red line between the residue and the ligand, and hydrogen bond is displayed by the single-oriented purple arrow. The figure was created by Maestro v. 11.4 (Schrödinger, LLC, New York, NY, 2017).

hydrogen contact between Asn2496 and 2,3-dihydropyridazin-3-one heterocycle. Ligand **14** (Fig. 6B) is bound in a very similar fashion to **13**, however, not displaying any characteristic interaction with the ribose binding site of ATP. Interestingly, 1*H*,5*H*-[1,2,4]triazolo[4,3-*b*]pyridazine of **14** is not in direct touch with lysine residues (Lys2327 and Lys2329). On the contrary, such type of interaction can be observed in the case of ligands **15** (Fig. 6C) and **16** (Fig. 6D). Classical π-π contacts are present between 6-nitronaphthalen-2-ol from **15** and 3,4-dihydro-2H-1,5-benzodioxepine from **16** with Trp2379 and Tyr2365, respectively. Ligand **17** is mostly lodged within the adenine-binding and ribose binding regions of ATP in ATR kinase staying outside the ATP-phosphate group binding site (Fig. 6E).

To conclude, our virtual screening has identified 17 different novel hits with potential affinity to interact with ATR kinase. Some of the structural features are common to more than one ligand like *ortho*-condensed pyrazole-based (or its triazole isosteres) tricyclic fragments present in compounds **2-6**, 6-amino-2-methyl-3,4-dihydro-2H-1,4-benzoxazin-3-one (for compounds **7** and **8**), or various lactam-containing scaffolds (e.g., **7**, **8**, **11**, **12**, **13**, and **16**).
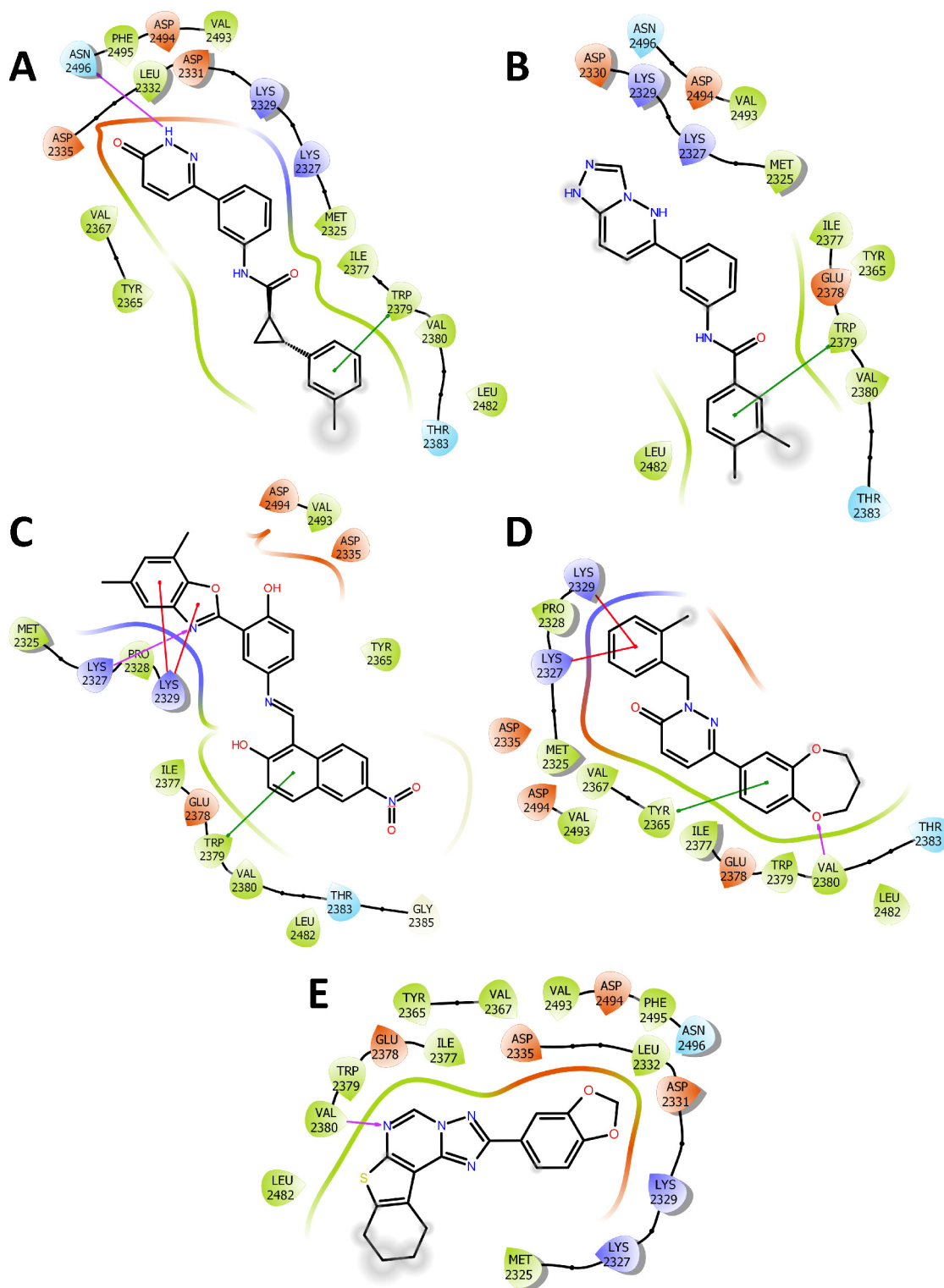
Figure 6. Two-dimensional representation of ligands **13-17** (A-**13**, B-**14**, C-**15**, D-**16**, E-**17**) bound to ATP-binding pocket of ATR kinase. Negatively charged area is colored by red residues or contour surrounding them, positively charged area by dark blue, hydrophobic interaction in green, polar interaction in light blue, solvent exposure via grey color, π-π stacking in green line between the residue and the ligand, cation-π in red line between the residue and the ligand, and hydrogen bond is displayed by the single-oriented purple arrow. The figure was created by Maestro v. 11.4 (Schrödinger, LLC, New York, NY, 2017).

In vitro screening of antiproliferative activity and chemosensitizing properties

To evaluate the antiproliferative effect of 17 compounds of interest, the primary screening was performed. Nine human cancer cell lines with various histotype (Jurkat, MOLT-4, A549, HT-29, PANC-1, A2780, HeLa, MCF-7, SAOS-2) and one non-tumor cell line (MRC-5) were exposed to each compound at a concentration of 10 µM for 48 hours. VE-821 (10 µM) and doxorubicin (1 µM) were used as positive controls. Heat map reflecting the changes in cell proliferation after treatment with single compound is displayed in Figure 7. Among the compounds tested, **1** and **8** stand out as the most active. Compound **1** showed a significant effect on A2780 cells, decreasing the proliferation to 35 %. Similarly, the effect of compound **8** was profound in A549 cells, where the proliferation dropped to 29 % of control cells. Contrary, the compound **14** boosted the proliferation in almost all cases. It can be speculated whether this is some nonspecific interaction between **14** with WST-1 assay (increase in absorption) or increased mitochondrial activity, especially in A2780.
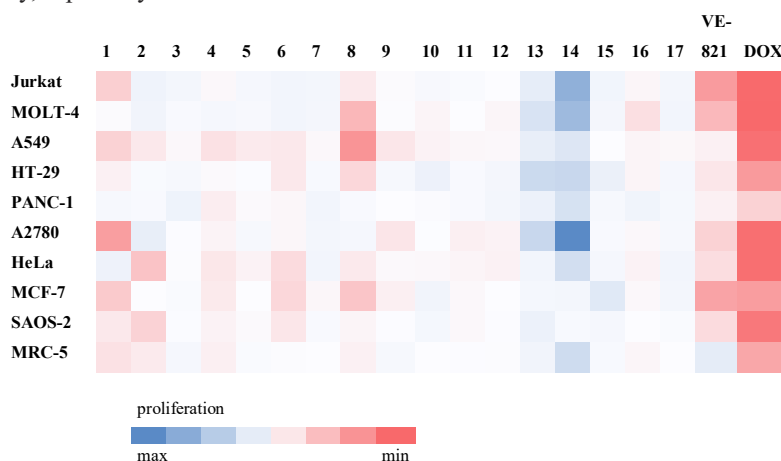
Figure 7. Antiproliferative capacity of tested compounds, VE-821 and doxorubicin as positive controls. Heat map represents effect of each compound on proliferation of 10 different cell lines. Cells were treated with the concentration of 10 µM for 48 hours, their proliferation was established by WST-1 assay and expressed as percentage of control cells (0.1% DMSO treated, proliferation 100 %).

To evaluate the overall antiproliferative capacity of each compound, the growth percentage was calculated. Mean growth percentage (GP) value is an average of 10 cell lines proliferation after 48 hours single-dose exposure of one individual compound at a concentration of 10 µM. Not surprisingly, compounds 1 and 8 displayed the lowest GP values of 78 and 75, respectively (Fig. 8).
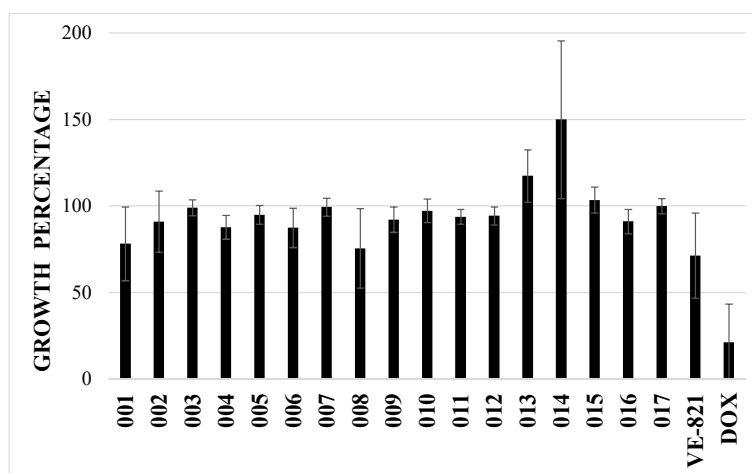
Figure 8. Mean growth percentage (GP) value was calculated for each compound as an average of 10 cell lines proliferation after 48 hours long single-dose exposure at a concentration of 10 µM.

For compound **1**, the GP ranged from 35 to 108 % of control cells, with A2780, MCF-7 and Jurkat being the most sensitive. Regarding compound **8**, the GP varied from 29 to 102 % of untreated cells, with A549, MOLT-4, MCF-7 being the most sensitive (Table 2).

Table 2. Mean growth percentage (GP) value was calculated for each compound as an average of 10 cell lines proliferation. Range of growth percentage and three most sensitive cell lines with proliferation values for compounds **1** and **8** are listed.

Compound	Mean GP	Range of GP	Most sensitive cell lines	% of control proliferation
1	78	35-108	A2780	35
			MCF-7	63
			JURKAT	66
8	75	29-102	A549	29
			MOLT-4	51
			MCF-7	60
VE-821	71	34-116	JURKAT	34
			MCF-7	39
			MOLT-4	52

According to the current knowledge, an inhibition of ATR kinase could sensitize cancer cells to other types of therapy (22). Therefore, we performed a set of experiments to assess the chemosensitizing properties of 17 compounds of interest toward cisplatin. First, we evaluated the sensitivity of each cell line to cisplatin (data not shown). For most of the cell lines, we selected the concentration that decreased the proliferation to 70-90 % of control cells and allowed us to monitor the chemosensitizing effect of inhibitors. Established cisplatin concentrations; 2 μM (MOLT-4, Jurkat, A2780), 10 μM (MCF-7, MRC-5) and 15 μM (A549, SAOS-2, PANC-1, HT-29, HeLa), were used in combination with 10 μM compounds **1-17** in all cell 10 cell lines. At the end of the incubation period (48 hours), WST-1 assay was carried out. Similarly, as in the primary screening, the proliferation of treated cells was compared to that of control cells (only solvent treated). Moreover, we compared the proliferation of cisplatin only treated cells to combination treated cells concomitantly with compound only treated cells to combination treated cells. Among the compounds tested, compound 1 proved chemo-sensitising effect in 5 cell lines tested (Jurkat, MOLT-4, A549, HeLa, MCF-7), compound **2** in 3 cell lines (MOLT-4, PANC-1, HeLa,), compound **4** in 4 cell lines (MOLT-4, HeLa, PANC-1, SAOS-2), compound **5** in 3 cell lines (MOLT-4, HeLa, SAOS-2), compound **6** in 5 cell lines (MOLT-4, A549, PANC-1, HeLa, SAOS-2), compound **8** in 1 cell line (MCF-7), compound **9** in 1 cell line (MOLT-4), compound **11** in 2 cell lines (MOLT-4, HeLa), compound **16** in 2 cell lines (MOLT-4, HeLa) and compound **17** in 3 cell lines (MOLT-4, SAOS-2, HeLa). The rest of compounds did not show chemisensitizing effect (Figure 9).

Conclusion

In this work, we performed a three-step in silico screening of novel potential ATR inhibitors and subsequent *in vitro* evaluation of antiproliferation capacity of 17 selected hits. First, 7 307 compounds were identified from ZINC Purchasable ligand library based on their pharmacophore resemblance to VX-970, a standard ATR inhibitor. Further, the number of compounds was narrowed to 293 according to semi-flexible molecular modelling prediction, and finally 17 hits arose from ultimate flexible docking studies. Structural features mimicking binding pattern of VX-970 were established, some of them being common to more than one compound. Among the compounds tested, compounds **1** and **8** caused significant decrease in proliferation to 35 % and 29 % respectively, compared to only solvent treated cells. Moreover, 10 of 17 compounds tested proved chemosensitizing effect, that was established by cisplatin co-treatment. Taking together, we described a set of novel potential inhibitors with chemosensitizing properties suitable for further evaluation of anticancer properties or representing a promising pattern for subsequent structural modifications.
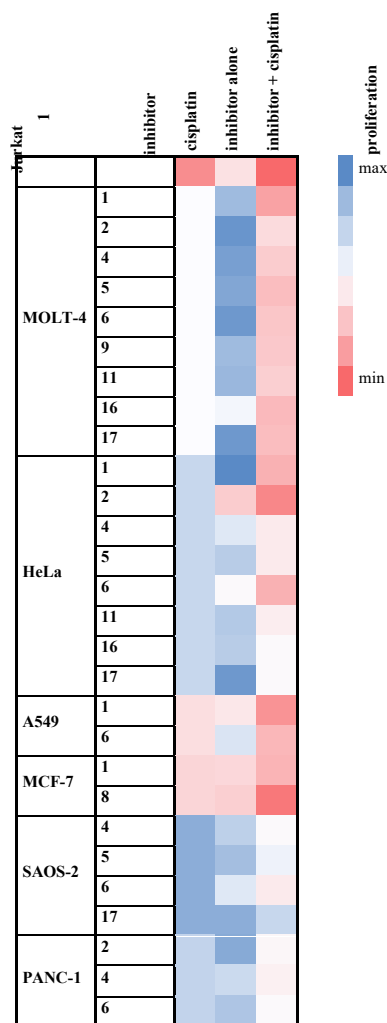
Figure 9. Chemo-sensitising properties of tested compounds. Cells were treated either with the inhibitors in concentration of 10 μM or cisplatin (concentration from 2 to 15 μM according to the cell sensitivity) or combination of both for 48 hours, their proliferation was established by WST-1 assay and expressed as percentage of control cells (0.1% DMSO treated, proliferation 100%).

Experimental section

Virtual screening and hit validation

The virtual screening campaign was done in three steps: pharmacophoric search and two molecular docking steps. The pharmacophore models were designed based on set of known ATR inhibitors as templates – *N,N*-dimethyl-4-[(6R)-6-methyl-5-(1H-pyrrolo[2,3-*b*]pyridin-4-yl)-4,5,6,7-tetrahydropyrazolo[1,5-*a*]pyrazin-3-yl]benzenesulfonamide, AZD6738, 3-amino-6-(4-((1-(dimethylamino)propan-2-yl)sulfonyl)phenyl)-N-phenylpyrazine-2-carboxamide (29), and *N,N*-dimethyl-4-[(6R)-6-methyl-5-(1H-pyrrolo[2,3-*b*]pyridin-4-yl)-4,5,6,7-tetrahydropyrazolo[1,5-*a*]pyrazin-3-yl]benzenesulfonamide (30). The poses of ligands were taken from the co-crystal structures – PDB IDs: 4WAF (30), 5UK8 (29), 5UKJ (29), and 5UL1 (29). The software Chimera aligned their crystallographic structures. The on-line environment of ZINCPharmer was used for building the pharmacophore models and for screening the ZINC database (ZINC Purchasable, last update 12/20/14) (28). A total of 6 models were used in total. All of them contained at least two aromatic features and two hydrogen bond acceptors. Some models included a hydrophobic region or a hydrogen bond donor. Each model included a minimum of five features. These screenings gave in total unique 7,307 hits.

The second phase used all the unique hits as ligands for molecular docking. Their 3D structures were built and converted into pdbqt-format by software OpenBabel (v. 2.0.2) (31). The receptor structure was gained from the RCSB database (PDB ID 5YZ0: Cryo-EM Structure of human ATR-ATRIP complex; 4.7 Å). It was prepared for the docking by the function DockPrep by the software Chimera (v. 1.14) (32) and MGLTools (v. 1.5.4.) (33). The semi-flexible docking calculations were done by Vina (v. 1.1.2) with flexible ligands and the rigid receptor (34).

A total of 293 hits were selected for the third phase. They were docked against the receptor structure PDB ID 5YZ0 by Vina software. The ligands and the eight receptor residues were set as flexible in this phase. Each ligand was docked 20 times and then manually inspected to find the optimal pose.

In vitro screening of antiproliferative activity

Selected human tumor and non-tumor cell lines Jurkat (acute T cell leukemia), MOLT-4 (acute lymphoblastic leukemia), A549 (lung carcinoma), HT-29 (colorectal adenocarcinoma), PANC-1 (pancreas epithelioid carcinoma), A2780 (ovarian carcinoma), HeLa (cervix adenocarcinoma), MCF-7 (breast adenocarcinoma), SAOS-2 (osteosarcoma) and MRC-5 (normal lung fibroblasts) were purchased from either ATCC (Manassas, USA) or Sigma-Aldrich (St. Louis, USA) and cultured according to the provider´s culture method guidelines. All cell lines were maintained at 37 °C in a humidified 5% carbon dioxide and 95% air incubator. Cells in the maximum range of either 10 passages for primary cell line (MRC-5), or in the maximum range of 20 passages for cancer cell lines (Jurkat, MOLT-4, A549, HT-29, PANC-1, A2780, HeLa, MCF-7 and SAOS-2) and in an exponential growth phase were used for this study.

Each cell line was seeded at previously established optimal density (1.10^3 to 50.10^3 cells per well) in a 96-well plate (TPP, Trasadingen, Switzerland) and cells were allowed to settle overnight. Cells were treated for 48 hours with compounds in the final concentration of 10 µM. Doxorubicin (Sigma-Aldrich, St. Louis, USA), at a concentration of 1 µM, was used as a positive control. At the end of the cultivation period, the WST-1 proliferation assay (Roche, Basel, Switzerland) was performed according to the manufacturer´s protocol and the absorbance was measured using a Tecan Spark (Tecan, Männedorf, Switzerland). Each value is the mean of three independent experiments and represents the percentage of proliferation 0.1% DMSO mock treated control cells (100%). The growth percentage (GP) value was calculated for each compound tested. GP represents the mean of the proliferation decrease in percent of all the 10 cell lines treated with the same compound.

To evaluate the chemo-sensitising effect of compounds, each cell lines was treated with increasing concentration of cisplatin in order to set the optimal concentration for each cell line. According to the data obtained, 3 concentrations of cisplatin were selected for combination assays: 2 µM (MOLT-4, Jurkat, A2780), 10 µM (MCF-7, MRC-5) and 15 µM (A549, SAOS-2, PANC-1, HT-29, HeLa). Cells were treated for 48 hours with the compound in the concentration of 10 µM and cisplatin in appropriate concentration. Again, at the end of the cultivation period, the WST-1 proliferation assay (Roche, Basel, Switzerland) was performed according to the manufacturer´s protocol and the absorbance was measured using a Tecan Spark (Tecan, Männedorf, Switzerland). Each value is the mean of three independent experiments and represents the percentage of proliferation 0.1% DMSO mock treated control cells (100%). Difference between only cisplatin treated and combination treated cells was considered together with compound only treated and combination treated cells.

Supplementary Materials

The followings are available online, Figure S1. Antiproliferative capacity of tested compounds, VE-821 and doxorubicin as positive controls. Table S1. Antiproliferative capacity of tested compounds, VE-821 and doxorubicin as positive controls.

Author Contributions

D.M., *in vitro* evaluation; T.K., virtual screening, manuscript writing; L.G. and M.A., manuscript writing and critical reading; M.R. and J.K., study design and manuscript writing. All authors have read and agreed to the published version of the manuscript.

Data availability

The datasets generated during and/or analysed during the current study are available from the corresponding author on reasonable request.

Adherence to Ethical Standards

Not applicable.

Conflict of Interest Statement

Authors declare no conflict of interest.

References

1. Siegel RL, Miller KD, Fuchs HE, et al. Cancer Statistics, 2021. CA Cancer J Clin. 2021;71:7–33. https://doi.org/10.3322/caac.21654.
2. Hanahan D, Weinberg RA. Hallmarks of Cancer: The Next Generation. Cell 2011;144:646–74. https://doi.org/10.1016/j.cell.2011.02.013.
3. Housman G, Byler S, Heerboth S, et al. Drug resistance in cancer: an overview. Cancers. 2014;6:1769–92. https://doi.org/10.3390/cancers6031769.
4. Dasika GK, Lin S-CJ, Zhao S, et al. DNA damage-induced cell cycle checkpoints and DNA strand break repair in development and tumorigenesis. Oncogene. 1999;18:7883–7899. https://doi.org/10.1038/sj.onc.1203283.
5. Andrs M, Korabecny J, Nepovimova E, et al. Small Molecules Targeting Ataxia Telangiectasia and Rad3-Related (ATR) Kinase: An Emerging way to Enhance Existing Cancer Therapy. Curr Cancer Drug Targets 2016;16:200–208. https://doi.org/10.2174/1568009616031602206122927.
6. Cimprich KA, Cortez D. ATR: an essential regulator of genome integrity. Nat Rev Mol Cell Biol. 2008;9:616–627. https://doi.org/10.1038/nrm2450.
7. Nam EA, Cortez D. ATR signalling: more than meeting at the fork. Biochem J. 2011;436:527–536. https://doi.org/10.1042/BJ20102162.
8. Halazonetis TD, Gorgoulis VG, Bartek J. An oncogene-induced DNA damage model for cancer development. Science. 2008;319:1352–1355. https://doi.org/10.1126/science.1140735.
9. Menezes DL, Holt J, Tang Y, et al. A synthetic lethal screen reveals enhanced sensitivity to ATR inhibitor treatment in mantle cell lymphoma with ATM loss-of-function. Mol Cancer Res. MCR 2015;13:120–129. https://doi.org/10.1158/1541-7786.MCR-14-0240.
10. Vendetti FP, Lau A, Schamus S, et al. The orally active and bioavailable ATR kinase inhibitor AZD6738 potentiates the anti-tumor effects of cisplatin to resolve ATM-deficient non-small cell lung cancer *in vivo*. Oncotarget. 2015;6:44289–44305. https://doi.org/10.18632/oncotarget.6247.
11. Reaper PM, Griffiths MR, Long JM, et al. Selective killing of ATM- or p53-deficient cancer cells through inhibition of ATR. Nat Chem Biol. 2011;7:428–430. https://doi.org/10.1038/nchembio.573.
12. Foote KM, Blades K, Cronin A, et al. Discovery of 4-{4-[(3R)-3-Methylmorpholin-4-yl]-6-[1-(methylsulfonyl)cyclopropyl]pyrimidin-2-yl}-1H-indole (AZ20): a potent and selective inhibitor of ATR protein kinase with monotherapy in vivo antitumor activity. J Med Chem. 2013;56:2125–2138. https://doi.org/10.1021/jm301859s.

13. Hall AB, Newsome D, Wang Y, et al. Potentiation of tumor responses to DNA damaging therapy by the selective ATR inhibitor VX-970. Oncotarget. 2014;5:5674–5685. https://doi.org/10.18632/oncotarget.2158.
14. Weber AM, Ryan AJ. ATM and ATR as therapeutic targets in cancer. Pharmacol Ther. 2015;149:124–138. https://doi.org/10.1016/j.pharmthera.2014.12.001.
15. Sanjiv K, Hagenkort A, Calderón-Montaño JM, et al. Cancer-Specific Synthetic Lethality between ATR and CHK1 Kinase Activities. Cell Rep. 2016;17:3407–3416. https://doi.org/10.1016/j.celrep.2016.12.031.
16. Kim H, Xu H, George E, et al. Combining PARP with ATR inhibition overcomes PARP inhibitor and platinum resistance in ovarian cancer models. Nat Commun. 2020;11:1–16. https://doi.org/10.1038/s41467-020-17127-2.
17. Andrs M, Korabecny J, Jun D, et al. Phosphatidylinositol 3-Kinase (PI3K) and Phosphatidylinositol 3-Kinase-Related Kinase (PIKK) Inhibitors: Importance of the Morpholine Ring. J Med Chem. 2015;58:41–71. https://doi.org/10.1021/jm501026z.
18. Gurley KE, Kemp CJ. Synthetic lethality between mutation in Atm and DNA-PK(cs) during murine embryogenesis. Curr Biol CB. 2001;11:191–194. https://doi.org/10.1016/s0960-9822(01)00048-3.
19. Schoppy DW, Ragland RL, Gilad O, et al. Oncogenic stress sensitizes murine cancers to hypomorphic suppression of ATR. J Clin Invest. 2012;122:241–252. https://doi.org/10.1172/JCI58928.
20. Hammond EM, Dorie MJ, Giaccia AJ. Inhibition of ATR leads to increased sensitivity to hypoxia/reoxygenation. Cancer Res. 2004;64:6556–6562. https://doi.org/10.1158/0008-5472.CAN-04-1520.
21. Pires IM, Olcina MM, Anbalagan S, et al. Targeting radiation-resistant hypoxic tumour cells through ATR inhibition. Br J Cancer. 2012;107:291–299. https://doi.org/10.1038/bjc.2012.265.
22. Mei L, Zhang J, He K, et al. Ataxia telangiectasia and Rad3-related inhibitors and cancer therapy: where we stand. J Hematol OncolJ Hematol Oncol. 2019;12. https://doi.org/10.1186/s13045-019-0733-6.
23. Llona-Minguez S, Höglund A, Jacques SA, et al. Chemical strategies for development of ATR inhibitors. Expert Rev Mol Med. 2014;16:e10. https://doi.org/10.1017/erm.2014.10.
24. Gorecki L, Andrs M, Rezacova M, et al. Discovery of ATR kinase inhibitor berzosertib (VX-970, M6620): Clinical candidate for cancer therapy. Pharmacol Ther. 2020;210:107518. https://doi.org/10.1016/j.pharmthera.2020.107518.
25. Gorecki L, Andrs M, Korabecny J. Clinical Candidates Targeting the ATR–CHK1–WEE1 Axis in Cancer. Cancers. 2021;13:795. https://doi.org/10.3390/cancers13040795.
26. Rao Q, Liu M, Tian Y, et al. Cryo-EM structure of human ATR-ATRIP complex. Cell Res. 2018;28:143–156. https://doi.org/10.1038/cr.2017.158.
27. Walker EH, Pacold ME, Perisic O, et al. Structural determinants of phosphoinositide 3-kinase inhibition by wortmannin, LY294002, quercetin, myricetin, and staurosporine. Mol Cell. 2000;6:909–919. https://doi.org/10.1016/s1097-2765(05)00089-4.
28. Irwin JJ, Sterling T, Mysinger MM, et al. ZINC: A Free Tool to Discover Chemistry for Biology. J Chem Inf Model. 2012;52:1757–1768. https://doi.org/10.1021/ci3001277.
29. Lu Y, Knapp M, Crawford K, et al. Rationally Designed PI3Kα Mutants to Mimic ATR and Their Use to Understand Binding Specificity of ATR Inhibitors. J Mol Biol. 2017;429:1684–1704. https://doi.org/10.1016/j.jmb.2017.04.006.
30. Barsanti PA, Aversa RJ, Jin X, et al. Structure-Based Drug Design of Novel Potent and Selective Tetrahydropyrazolo[1,5-a]pyrazines as ATR Inhibitors. ACS Med Chem Lett. 2015;6:37–41. https://doi.org/10.1021/ml500353p.
31. O'Boyle NM, Banck M, James CA, et al. Open Babel: An open chemical toolbox. J Cheminformatics 2011;3:33. https://doi.org/10.1186/1758-2946-3-33.
32. Pettersen EF, Goddard TD, Huang CC, et al. UCSF Chimera--a visualization system for exploratory research and analysis. J Comput Chem. 2004;25:1605–1612. https://doi.org/10.1002/jcc.20084.
33. Morris GM, Huey R, Lindstrom W, et al. AutoDock4 and AutoDockTools4: Automated docking with selective receptor flexibility. J Comput Chem. 2009;30:2785–2791. https://doi.org/10.1002/jcc.21256.
34. Trott O, Olson AJ. AutoDock Vina: improving the speed and accuracy of docking with a new scoring function, efficient optimization and multithreading. J Comput Chem. 2010;31:455–461. https://doi.org/10.1002/jcc.21334.